ADVANCES IN ATMOSPHERIC SCIENCES, VOL. 26, NO. 3, 2009, 493–502

# Impacts of Land Surface and Sea Surface Temperatures on the Onset Date of the South China Sea Summer Monsoon

LIU Peng[1,2] (刘 鹏), QIAN Yongfu[*1] (钱永甫), and HUANG Anning[1] (黄安宁)

[1] *Department of Atmospheric Sciences, Nanjing University, Nanjing* 210093

[2] *Key Laboratory of Meteorological Disaster of Ministry of Education, Nanjing University of Information Science and Technology, Nanjing* 210044

(Received 20 January 2008; revised 1 August 2008)

**ABSTRACT**

The present study analyzes the differences in spatial and temporal variations of surface temperatures between early and late onset years of the South China Sea summer monsoon (SCSSM). It is found that when the land surface temperature north of 40°N is lower (higher) and the sea surface temperature over the South China Sea-western North Pacific (SCS-WNP) is higher (lower) in winter, the onset of the SCSSM begins earlier (later). When the land surface temperature north of 40°N is higher (lower) and the sea surface temperature over the SCS-WNP is lower (higher) in spring, the onset of the SCSSM occurs earlier (later). The reason why the anomalies of the land surface temperatures north of 40°N can influence the atmospheric circulation is investigated by analysis of the wind and temperature fields. In order to verify the mechanisms of influence over the land and sea surface temperature distribution patterns and test the ability of the $p$-$\sigma$ regional climate model ($p$-$\sigma$ RCM9) to simulate the SCSSM onset, three types of years with early, normal, and late SCSSM onset are selected and the SCSSM regimes are numerically simulated. According to the results obtained from five sensitive experiments, when the land surface temperature is higher in the eastern part, north of 40°N, and lower in the western part, north of 40°N, and it rises faster in the eastern coastal regions and the Indian Peninsula, while the sea surface temperatures over the SCS-WNP are lower, the early onset of the SCSSM can be expected.

**Key words**: surface temperature, South China Sea summer monsoon, numerical simulations

**Citation**: Liu, P., Y. F. Qian, and A. N. Huang, 2009: Impacts of land surface and sea surface temperatures on the onset date of the South China Sea summer monsoon. *Adv. Atmos. Sci.*, **26**(3), 493–502, doi: 10.1007/s00376-009-0493-2.

## 1. Introduction

It is commonly believed that the tropical Asian summer monsoon onsets firstly in the South China Sea (SCS). The onset of the SCS Summer Monsoon (SCSSM) indicates the coming of the East Asian Summer Monsoon and the beginning of the rainy season in East China. The anomalies of the onset date and intensity of the SCSSM are associated with that of the atmospheric circulation and influences the weather and precipitation in East China. Many scientists have conducted different kinds of studies on the mechanism of the onset of the SCSSM. Wu and Zhang (1998) pointed out that the Bay of Bengal (BOB) monsoon was directly linked to the thermal as well as the mechanical forcing of the Tibetan Plateau. It then generated a favorable environment for the SCSSM onset. Wu and Wang (2001) pointed out the role of condensational heating over South China in the reversal of the tropospheric meridional temperature gradient in the South China Sea sector and the SCSSM onset. Liu et al. (2003a,b) discussed the physical linking between the BOB monsoon onset and the SCSSM onset and found that the condensation heating over the north part of the SCS induced the reversal of the meridional temperature gradient in this region, and thus the onset of the SCSSM.

Qian et al. (2001) analyzed the time evolutions of

*Corresponding author: QIAN Yongfu, qianzh2@nju.edu.cn

the surface sensible heat (SH) fluxes in the tropical and subtropical regions of the SCS and in the Indian Peninsula, as well as their relations with the difference in the timing of the SCSSM and the Indian monsoon onset, and pointed out that the west-east contrasts of the SH fluxes in the middle latitudes were favorable to the earlier onset of the SCSSM compared to the Indian monsoon. By analyzing the sensible heat and latent heat fluxes in 1998, Wang and Qian (2001) found that the continuous distribution of sensible heat from south to north in the meridional region of the Indo-China Peninsula was important for the earliest onset of the summer monsoon in the SCS.

In addition to the meridional difference of solar radiation and the thermal effect of the Tibetan Plateau mentioned above, the land-sea thermal contrast is also an important factor influencing the onset time of the SCSSM, which can be reflected by land surface and sea surface temperatures. In the seasonal transition from spring to summer, the contributions of land and sea thermal conditions to the land-sea thermal contrast are different because of their different rates of temperature rise. Based on the analysis of different variations of land and sea surface temperatures and their influence on the atmospheric general circulation in the early and late onset years of the SCSSM, respectively, an important factor influencing the onset time of the SCSSM is revealed in this paper.

## 2. Data and calculation methods

The atmospheric data used in this study is taken from the National Centers for Environmental Prediction (NCEP)/National Center for Atmospheric Research (NCAR) reanalysis for the period 1948–2002. This research makes use of the daily data and pentad-mean data of 55 years. There are many definitions of the SCSSM onset index (He et al., 2001). Figure 1 shows the 55-year onset time from 1948 to 2002 with the SCS (0°–10°N, 105°–120°E) Summer Monsoon Index defined by Yao and Qian (2001) using potential vorticity at 850 hPa. The SCSSM Index is defined as follows:

$$P_m = \rho^{-1}\zeta \cdot \nabla\theta_{\rm se}\,, \tag{1}$$

$$(\Delta P_{\rm m})_j = (\overline{P}_{\rm m})_j - \sum \overline{(P_{\rm m})_j}/m\,, \tag{2}$$

$$I_{\rm pm} = (\Delta P_{\rm m})/\sqrt{\sum (\Delta P_{\rm m})_j^2/m}\,, \tag{3}$$

where "—" is the space average, $\theta_{\rm se}$ is the equivalent potential temperature, $P_{\rm m}$ is the vertical component of moisture potential vorticity in the grid point, $j$ is the pentad, $m$ is the total number of pentads, and $I_{\rm pm}$ is the standardized vorticity monsoon index. It well represents the onset time of the SCSSM as compared with other indexes, with the mean onset time in the 28th pentad and a standard deviation of 2.1 pentads. The years with the onset time at and before the 26th pentad are defined as early onset years of the SCSSM (EYM), while the years with an onset time at and after the 30th pentad are defined as late onset years of the SCSSM (LYM). So, there are 15 EYMs and 14 LYMs during the period 1948–2002. The data in the former 15 years and the latter 14 years were chosen for composite analysis pentad by pentad, respectively. The mean of 55 years is considered as a normal onset year (NYM).

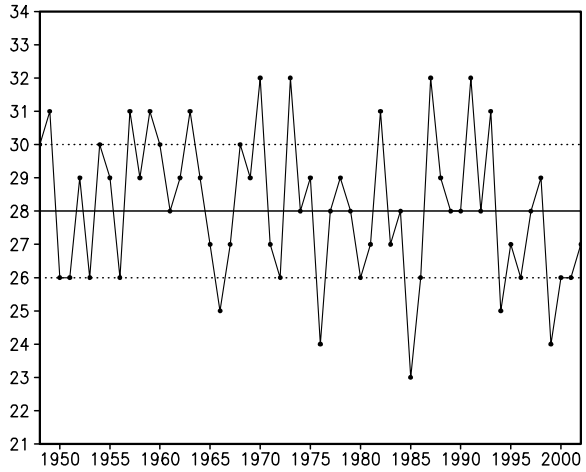


**Fig. 1.** The SCSSM onset time during the period from 1948 to 2002 (Units: pentad).

## 3. Analysis on differences of spatial and temporal variations between the EYM and the LYM

Firstly, differences between the pentad-mean composite surface temperatures in the EYM and the LYM pentad by pentad are computed and analyzed by means of EOF. Therefore, there is a surface temperature differences field between the EYM and the LYM, pentad by pentad, with 73 pentads at each grid point and the data during 1–48 pentads are used for the EOF analysis. It is the aim of the EOF analysis that the surface temperature differences between the EYM and the LYM be found in various spaces and various times. So, these differences between the EYM and the LYM are very possible to influence the onset date of SCSSM. The first and second EOF modes account for 30% and 10% of the total variance, respectively. Figure 2a shows the negative EOF value center is loca-

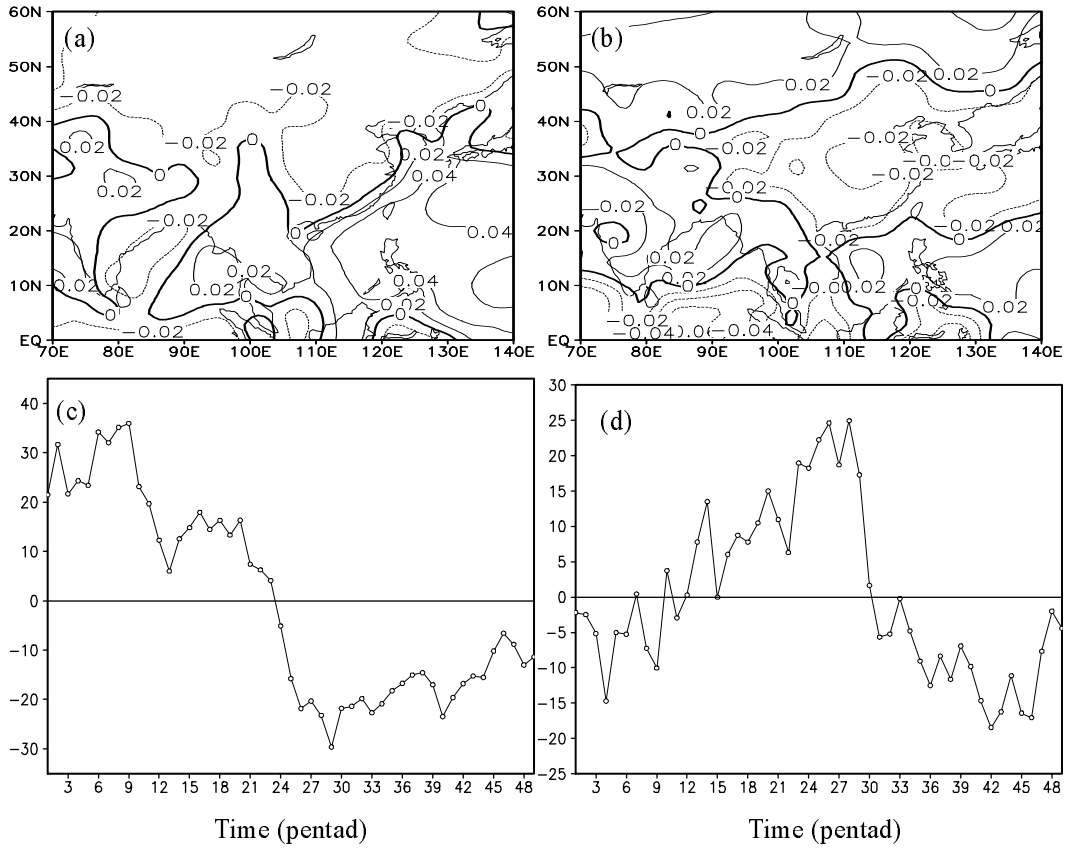


**Fig. 2.** The EOF analysis of the differences of land and sea surface temperatures between the EYM and the LYM: (a) 1st mode, (b) 1st temporal coefficients, (c) 2nd mode, and (d) 2nd temporal coefficients.

ted on land, north of 40°N, and the positive center is in the sea. It is shown that the difference of the land-sea thermal contrast between the EYM and the LYM is quite obvious. Before the 24th pentad, the temporal coefficients of the first EOF mode are positive. The characteristics of the surface temperature differences between the EYM and the LYM averaged over 1–24 pentads shows that the land north of 40°N is colder in the EYM and warmer in the LYM, and the ocean is warmer in the EYM, and colder in the LYM, respectively, revealing the strong land-sea thermal contrast in the EYM and the weak land-sea thermal contrast in the LYM. The EOF1 time coefficient displays a quick change from positive to negative during 18–28 pentads. This indicates that the land surface temperature rises faster, whereas the sea surface temperature rises slower in the EYM than in normal years. As such, the land-sea thermal contrast is enhanced in the EYM. In the LYM, the land surface temperature rises slower and the sea surface temperature rises faster, and the land-sea thermal contrast is reduced. After the 24th pentad, the temporal coefficients are negative, therefore the land surface temperatures north of 40°N are higher and the sea surface temperatures over the SCS-WNP are lower in the EYM.

Because the variance of the second EOF mode is smaller, the second characteristic vector is regarded as a disturbance field overlapping the mean climate. Figures 2b and 2d show the second EOF mode and its temporal coefficients, different from those in the first mode. The second temporal coefficients are positive in the 16th–29th pentads. During this time, the positive EOF values are located along 45°N and 20°N, and the negative ones in the East China coastal regions. The characteristics of the surface temperature differences between the EYM and the LYM averaged in the 18th–29th pentads shows that the surface temperatures in regions along 45°N and 20°N are higher and lower, respectively, while the surface temperatures in the East China coastal regions and in the equatorial region between 70°–100°E are lower.

The above case shows that there are strong winter monsoons in the EYM and weak winter monsoons in the LYM. It is consistent with numerous other research results, and Wu and Huang (2001) pointed out that the strong winter monsoon may impel the early

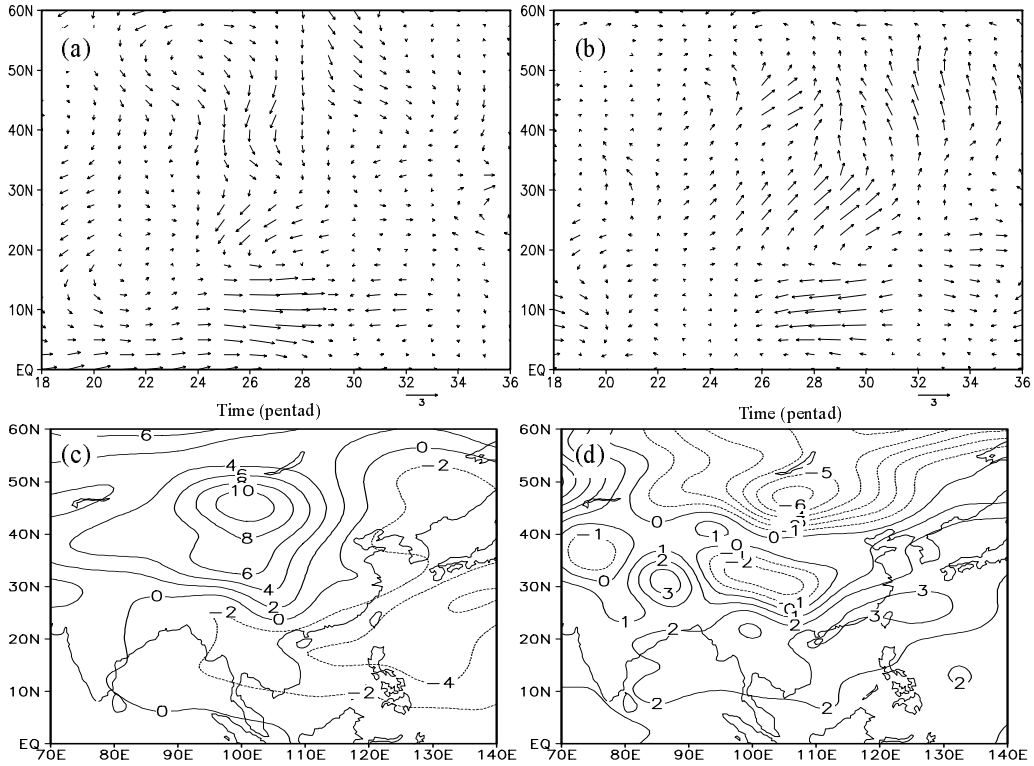


**Fig. 3.** Time-latitude cross-sections of wind anomaly fields in (a) the EYM and (b) the LYM at 850 hPa along 110°–120°E (Units: m $s^{-1}$); height anomaly fields in (c) the EYM and (d) the LYM at 850 hPa.

onset of the SCSSM. It is a possible reason: the strong (weak) winter monsoon in the EYM (LYM) strengthens the northerly (southerly) wind anomaly, and the northerly (southerly) wind anomaly is beneficial to decrease (increase) with the rate of SSTs during the 18th–28th pentads. It stands a good chance that the strong winter monsoon results in a high heating rate of the 1st and low heating rate of the SSTs. Furthermore, it is also an important condition for the early onset of the SCSSM that the land-sea thermal contrast is greater in April to May in the EYM than in the LYM.

## 4. The atmospheric circulation anomalies responsible for influencing the onset time of the SCSSM

The influence of land and sea surface temperatures on the onset time of the SCSSM is mostly by means of inducing anomalies of atmospheric circulation. With the onset of the SCSSM, there are obvious time variations in the low-level wind, high-level geopotential height, temperature, humidity, and vertical motion fields in South and Southeast Asia. In the following section, we will analyze the internal relations between these variations and the influence of land and sea surface temperatures on them.

### 4.1 *Analysis of wind and height fields in the EYM and in the LYM*

Figures 3a and 3b show time-latitude cross-sections of the wind anomaly field at 850 hPa in the EYM and the LYM along 110°–120°E. It can be seen from Fig. 3a that there is a westerly wind anomaly near the equator as early as the 18th pentad because cross-equatorial flow is stronger in the EYM (Li and Wu, 2003). It also can be seen that a northerly wind anomaly appears in the area from 20°N to the north in the 18th pentad, and it increases gradually during the 24th–28th pentads. As shown in Fig. 3b, an easterly wind anomaly appears in the SCS in the 26th pentad of the LYM, while a southerly wind anomaly commences in the region north of 20°N from the 20th pentad, which increases gradually during the 25th–30th pentads.

In the seasonal transition from spring to summer, air pressure increases on both the sea and land, but the rising rates of air pressure on the sea and land are inconsistent in the EYM and LYM. Figures 3c and 3d depict the geopotential height anomaly fields at 850 hPa averaged in the 18th–28th pentads in the EYM and the LYM. It shows that there are positive pressure

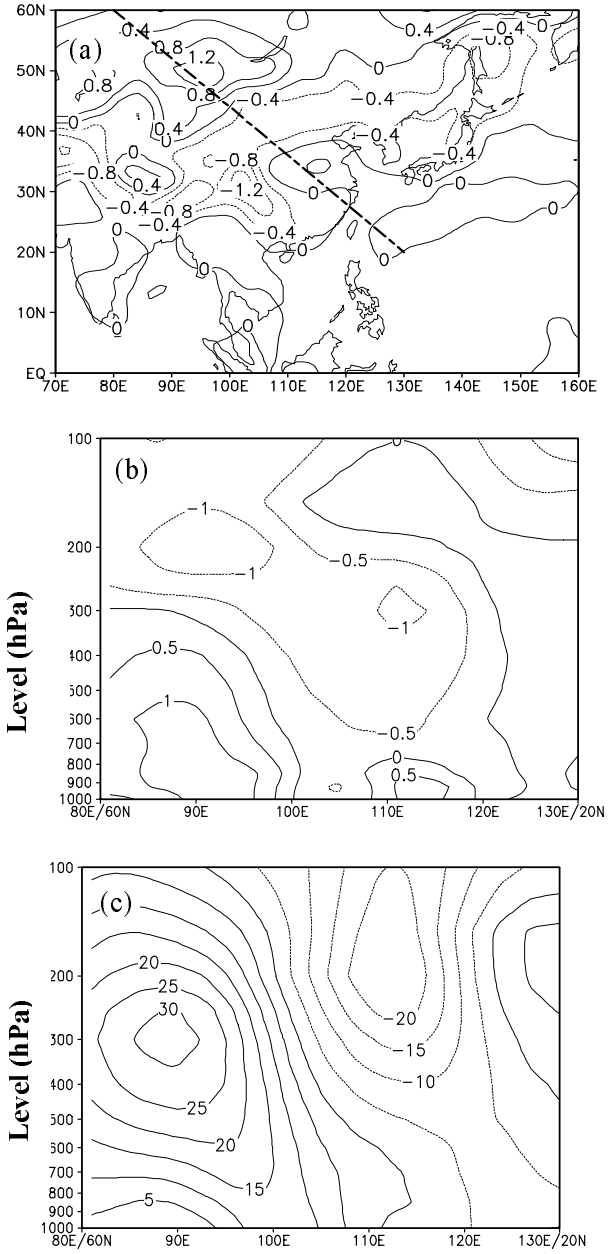


**Fig. 4.** (a) The surface temperature differences between the EYM and the LYM averaged in the 18th–28th pentads (Units: °C); vertical cross-section of (b) air temperature field and (c) height field differences between the EYM and the LYM along from (60°N, 80°E) to (20°N, 130°E) averaged in the 18th–28th pentads.

differences over land and negative pressure differences over the sea, which indicates that low-level air pressure elevates faster over land and slower over the sea in the EYM, and vice versa in the LYM. There is an anticyclonic difference on the left side of 115°E and a cyclonic difference on the right side of 115°E in the EYM (Fig. 3c). Since the wind moves mainly along the isobar, the northerly wind difference in Fig. 3a can then be explained. With the same reason, the southerly wind difference (Fig. 3b) in the LYM can be explained, too.

### 4.2 *Influence of land and sea surface temperatures on the general circulation of the atmosphere*

Figure 4a shows the surface temperature difference between the EYM and the LYM averaged in the 18th–28th pentads. A positive surface temperature difference appears to the north of 40°N and negative surface temperature differences appear over the SCS-WNP. The surface temperature difference is one of the important reasons why there is an obvious difference in the 850 hPa geopotential height fields between the EYM and the LYM, discussed previously. Figures 4b and 4c show the vertical cross-sections of air temperature and geopotential height field differences between the EYM and the LYM along the line from (60°N, 80°E) to (20°N, 130°E) averaged in the 18th–28th pentads. It is found that there is a high air temperature in the mid-low troposphere over the middle-high latitudes, corresponding to the warm center of the land surface temperatures north of 40°N in Fig. 4b. The strong ascending motion in the lower atmosphere (not shown) over this area is one of the primary causes why air temperature in the mid-low troposphere rises. In the vertical cross-section of the height field, it reflects the result of static balance, displaying that the positive pressure center at 300 hPa over the middle-high latitudes corresponds to the higher air temperature in the low troposphere and lower air temperature in the upper troposphere.

Received solar radiation differs with latitudes. The energy exchange between the middle-high latitudes and the low latitudes is mostly implemented by the Hadley circulation and the Ferrel circulation, which are usually described by the mass of stream functions, the calculation method of which can be found in Oort and Yienger (1996) and Gong et al. (2002). In the seasonal transition from spring to summer, there is a process that receivable solar radiation increases gradually in the Northern Hemisphere with the northward shift of the subsolar point, and the Hadley circulation and the Ferrel circulation become weaker and weaker. Figures 5a and 5b respectively show the mass stream functions in the normal years and those differences between the EYM and the LYM averaged in the 18th–28th pentads. Comparing the two figures, we can see that both the Hadley circulation and the Ferrel circulation weaken earlier in the EYM than in the LYM. The Hadley circulation and the Ferrel circulation described by the mass stream functions are the result of the global zonal mean. We can find the explanation

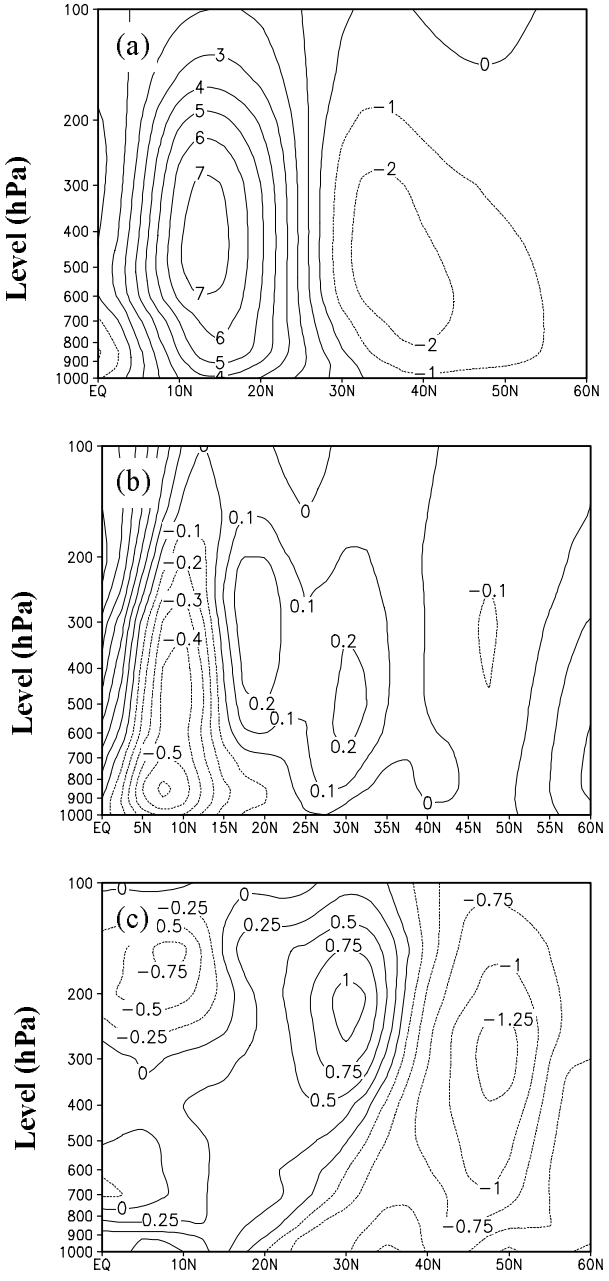


**Fig. 5.** Mass stream functions of (a) normal years or (b) difference between the EYM and the LYM averaged in the 18th–28th pentads (Units: $10^{10}$ kg s$^{-1}$); and (c) the latitude-height drawing of $v$ field difference between the EYM and the LYM along 110°–140°E averaged in the 18th–28th pentads (Units: m s$^{-1}$).

from Fig. 5c whether the circulation system in East Asia corresponds to the situation or not. Figure 5c is the latitude-height drawing of the meridional wind field difference between the EYM and the LYM along 110°–140°E averaged in the 18th–28th pentads. The drawing shows that the southerly wind difference appears in the lower latitude region and the northerly wind difference appears from 30°N to the north in the lower troposphere, whereas the northerly wind and southerly wind differences respectively appear in the lower latitudes region and in the area of 30°–50°N in the upper troposphere. The meridional wind field difference, which is opposite in sign between the upper troposphere and the lower troposphere, is a reflection of the weakened Hadley and Ferrel circulations.

According to the results mentioned above, we can arrive at some conclusions. The land surface temperatures in the middle-high latitudes rise rapidly during the 18th–28th pentads in the EYM, and the air temperatures increase quickly in the low-middle troposphere due to the heating effect of the underlying surfaces. Consequently, there is a deep positive pressure difference in the upper troposphere. The existence of a positive pressure difference over the land and a negative pressure difference over the sea results in the appearance of a northerly wind anomaly in the low troposphere of the middle latitudes and the weakened Ferrel circulation at the same time, which influences the Hadley circulation and makes it weakened as well. The weakening of the Hadley circulation leads to the existence of a southerly wind difference in the low troposphere of the low latitudes, which is an important signal of the SCSSM onset. So, these conditions impel the SCSSM onset earlier. On the contrary, the land surface temperatures in middle-high latitudes rise slowly during the 18th–28th pentads in the LYM. The situation impelling the SCSSM onset is on the contrary to that in the EYM.

## 5. Numerical simulations analysis

### 5.1 *Model description and numerical experiment schemes*

The $p$-$\sigma$RCM9 regional climate model used in this study is based on a primitive equation model with a $p$-$\sigma$ vertical coordinate system. It has 9 vertical atmospheric layers with a horizontal resolution of 1° × 1°. The pressure coordinate is used above 400 hPa with four uniform layers. Below 400 hPa, $\sigma$ coordinates are adopted. Four $\sigma$ layers are uniformly divided with $\Delta\sigma$=0.25, and only one layer is defined as the atmospheric boundary layer with a 50 hPa thickness in the $\sigma_b$ coordinate. The model domain is from 9°S to 59°N in latitude and from 70°E to 140°E in longitude, including the Tibetan Plateau, the Bay of Bengal, the South China Sea, and part of the western Pacific. The model includes a planetary boundary-layer parameterization process, Kuo-type cumulus parameterization scheme (Anthes, 1977; Kuo and Qian, 1981, 1982) and

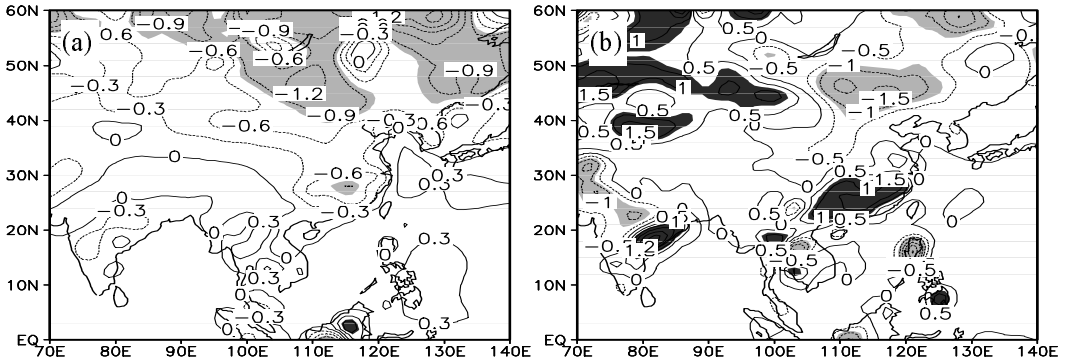


**Fig. 6.** The simulated surface temperature differences between EO-EXP and LO-EXP. (Units: °C): (a) averaged in the 1st–18th pentads; (b) averaged in the 19th–28th pentads (black for the region over 0.8°C and gray for the region under −0.8°C).

a detailed atmospheric radiation process. The *p*-$\sigma$RCM9 and the previous versions have been extensively and successfully used to simulate the large-scale circulations and to investigate the impacts of the air-sea feedback on the atmospheric circulations (Wang and Qian, 2002; Zhang and Perrie, 2001; Ren and Qian, 2005).

In this paper, two groups of numerical experiments have been performed. The first one includes three simulations for the early, late, and normal onset of the SCSSM, respectively named EO-EXP, LO-EXP, and NO-EXP correspondingly. The initial and boundary conditions, including wind, air temperature, specific humidity, and geopotential height fields, are specified by the National Centers for Environmental Prediction/National Center for Atmospheric Research (NCEP/NCAR) reanalysis monthly mean data which are composed of the respective early, late, and normal onset years of the SCSSM, and SST forcing is provided by the NCEP/NCAR re-analysis monthly mean SST in the corresponding years. Each run has been integrated from 17 December to 31 December of the next year. We analyzed the last 365 days of simulations. This group of numerical experiments is designed to validate the model's performance in simulating the early and late onset of the SCSSM. The second group has 5 numerical experiments, as shown below:

(1) EXP1: LSTs north of 40°N are replaced by that in the EYM;

(2) EXP2: LSTs south of 40°N are replaced by that in the EYM;

(3) EXP3: All SSTs are replaced by that in the EYM;

(4) EXP4: All LSTs are replaced by that in the EYM;

(5) EXP5: All STs are replaced by that in the EYM.

All experiments have the same initial and boundary conditions, which are offered by the composed NCEP/NCAR data in the LYM, but the surface temperatures in different regions in the LYM are replaced with that in the EYM. This group of experiments is designed for studying the impacts of the surface temperatures in different regions at the onset of the SCSSM.

### 5.2 *The simulation results for the onset date of the SCSSM*

The SCSSM onset dates in the EO-EXP, NO-EXP, and LO-EXP are respectively the 24th, the 26th, and the 29th pentad and very close to the real onset dates, and basically represent the difference of the SCSSM onset date between the EYM and the LYM, but about 1–2 pentads earlier.

Figure 6 shows the simulated surface temperature differences between EO-EXP and LO-EXP. As shown in Fig. 6a, it is noted that the *p*-$\sigma$RCM9 regional climate model can fairly reproduce the characteristics of the surface temperature differences between the EYM and the LYM averaged in the 18th–28th pentads, which shows colder to the north over land and a warmer ocean in the EYM. Figure 6b shows that the model also gets the characteristic of the surface temperature differences between the EYM and the LYM averaged in the 19th–28th pentads: the warm regions are located in the north over land and the East China coastal regions, while the cold regions appear over northeast China and the SCS-WNP.

Based on the analysis above, we may conclude that the *p*-$\sigma$RCM9 regional climate model can reproduce well the onset date of the SCSSM and the surface temperature differences between the EYM and the LYM.

Figure 7 shows the differences of air temperature, geopotential height, and wind fields between the five sensitivity experiments and the LO-EXP at 850 hPa averaged in the 18th–28th pentads. In EXP1, the land

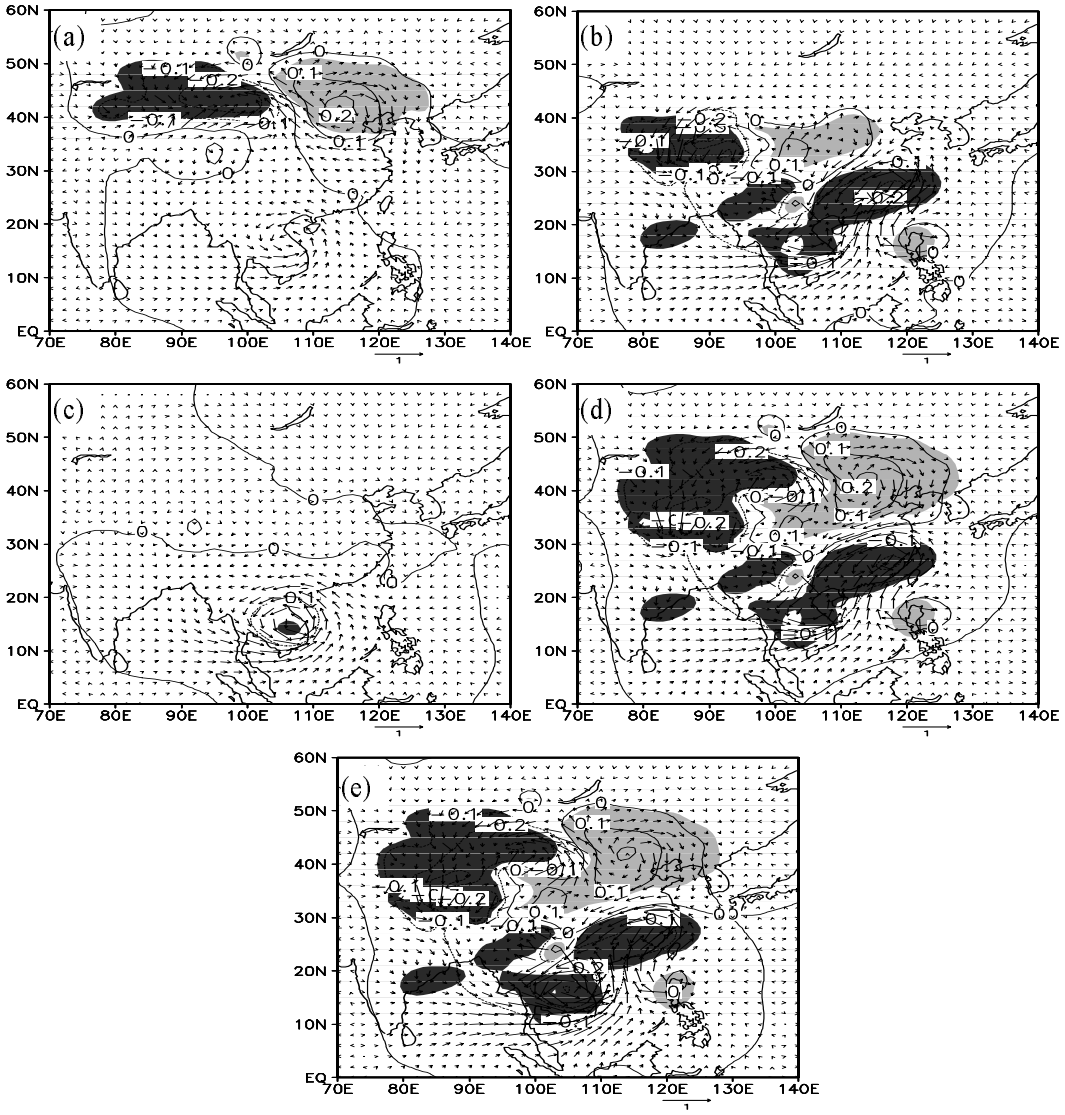


**Fig. 7.** (a) EXP1, (b) EXP2, (c) EXP3, (d) EXP4, and (e) EXP5. The air temperature, geopotential height, and wind differences between the five sensitivity experiments and the LO-EXP at 850 hPa averaged in the 18th–28th pentads (Units: dagpm) (black for the region over 0.15°C and gray for the region under −0.15°C).

surface temperature north of 40°N is replaced with that in the EYM. As shown in Fig. 7a, under the influence of the surface temperature distribution over the land north of 40°N (warmer in the east and colder in the west), there are positive air temperature differences and negative pressure differences in the east, and vice versa in the west, and a negative pressure difference center forms on the Indochina peninsula. The northerly wind difference in the mid-latitudes between 95°E and 110°E strengthens the anticyclone in the west north of 40°N, which enhances the southerly wind in the mid-latitudes between 115°E and 125°E. For these reasons, the Ferrel circulation becomes weakened in the regions and it decreases the Hadley circulation, then the weakened Hadley circulation intensifies the southerly wind over the SCS.

The scheme, when land surface temperatures from 40°N to the south are replaced with that in the EYM, is adopted on EXP2. As shown in Fig. 7b, two positive air temperature difference centers are located over the BOB and the East China coastal region, respectively. The positive air temperature difference center over the BOB strengthens the westerly wind in the low latitudes. However, the cyclone over the East China coastal region strengthens the southwesterly wind over the SCS. Results from EXP3, shown in Fig. 7c, show

that only one small and positive temperature difference center appears over the Indochina peninsula, and the accompanying cyclone over this region reinforces the southwesterly wind over the SCS. Results from EXP4 in Fig. 7d have the characteristic of the sum of the situation in Figs. 7a and 7b. The situation of EXP5 in Fig. 7e is very similar to that in Fig. 7d, only the air temperature difference over the Indochina peninsula is more positive while the corresponding southwesterly wind is much stronger.

As mentioned above, it can be found that the influencing mechanism of the land regions north of 40°N is different to that south of 40°N on the SCSSM. However, the SCSSM breaks out earlier when there are warmer temperatures in the east over the land, colder temperatures to the west over the land north of 40°N, and the surface temperatures rapidly increase over the East China coastal region and the Indochina peninsula during the 18th–28th pentads. Furthermore, the low SSTs over the SCS-WNP during the 18th–28th pentads also can make the SCSSM break out earlier, but the land has a much more important effect than the ocean.

## 6. Conclusions and remarks

By the analysis and numerical simulations, it can be concluded:

(1) Through analysis of the differences of spatial and temporal variations between early and late onset years of the SCSSM by means of EOF, it is found that when the land surface temperatures north of 40°N are lower (higher) and the sea surface temperatures over the SCS-WNP are higher (lower) in winter, the onset of the SCSSM begins earlier (later). When the land surface temperatures north of 40°N and the Indian Peninsula are higher (lower) and the sea surface temperatures over the SCS-WNP are lower (higher) in spring, the onset of the SCSSM occurs earlier (later).

(2) After the wind and height fields and so on were investigated, the land surface temperatures in the middle-high latitudes rise rapidly during the 18th–28th pentads of the EYM. Due to the effect of heating from the underlying surfaces, the air temperature increases quickly in the low-middle troposphere too. There is deep positive pressure in the upper troposphere. The existence of a positive pressure difference over land and a negative pressure difference over the ocean results in the appearance of a northerly wind anomaly in the low troposphere of the middle latitudes and a weakened Ferrel circulation at the same time, which makes the Hadley circulation weakened as well. The weakening of the Hadley circulation leads to a southerly wind difference in the lower troposphere of the low latitudes, which is an important signal of the SCSSM onset. So, these conditions impel the SCSSM onset earlier. On the contrary, the land surface temperatures in the middle-high latitudes rise slowly during the 18th–28th pentads in the LYM. The situation impelling the SCSSM onset is contrary to that in the EYM.

(3) Through experiments and numerical simulations, the ability of the $p$-$\sigma$ regional climate model ($p$-$\sigma$RCM9) to simulate the SCSSM onset is tested. It is shown that the SCSSM onsets earlier when the land surface temperature anomalies are positive in the eastern part, north of 40°N, negative in the western part, when the land surface temperatures rise faster in the eastern coastal regions, and the Indian Peninsula and the SSTs rise slower over the SCS-WNP during the 18th–28th pentads.

Based on the pentad-mean data in this paper, the effects of land and sea surface temperatures on the SCSSM onset time is analyzed, but the daily variation is not involved. Land surface temperatures change rapidly and sea surface temperatures change slowly, so it is possible that some details affecting the SCSSM onset are ignored. Therefore, it is needed to possibly emphasize that diurnal variations of the different heating rates between the land and sea surface temperatures have various effects on the SCSSM onset.

***Acknowledgements.*** Thanks go to Dr. Z. F. Wang and Dr. D. Q. Huang for their support of this research. This work was supported by the National Natural Science Foundation of China under Grant No. 40675042.

## REFERENCES

Anthes, R. A., 1977: A cumulus parameterization scheme utilizing a one-dimensional cloud model. *Mon. Wea. Rev.*, **105**(3), 270–286.

Gong, Z.-S., P.-X. Wang, and J. Ma, 2002: Application of a simplified calculation scheme for mean meridional circulation mass stream function. *Journal of Nanjing Institute of Meteorology*, **25**(4), 328–333. (in Chinese)

He, J. H., Y. H. Ding, and H. M. Xu, 2001: *Determination of the Data of South China Sea Monsoon Onset and Monsoon Indices*. China Meteorological Press, Beijing, 123pp. (in Chinese)

Kuo, H. L., and Y. F. Qian, 1981: Influence of the Tibetan Plateau on cumulative and diurnal changes of weather and climate in summer. *Mon. Wea. Rev.*, **109**, 2337–2356.

Kuo H. L., and Y. F. Qian, 1982: Numerical simulation of the development of mean monsoon circulation in July. *Mon. Wea. Rev.*, **110**, 1879–1897.

Li, C. Y., and J. B. Wu, 2003: Important role of the somalian cross-equator flow in the onset of the South China Sea summer monsoon. *Chinese J. Atmos. Sci.*,

**26**(2), 185–192. (in Chinese)

Liu, Y. M., Z. L. Chen, and G. X. Wu, 2003a: Impact of the onset of the bay of Bengal monsoon on the onset of the South China Sea monsoon. Part I: A case study. *Acta Meteorologica Sinica*, **61**(1), 1–8. (in Chinese)

Liu, Y. M., Z. L. Chen, J. Y. Mao, and G. X. Wu., 2003b: Impact of the onset of the bay of Bengal monsoon on the onset of the South China Sea monsoon. Part II: Numerical experiments. *Acta Mereorologica Sinica*, **61**(1), 10–21. (in Chinese)

Oort, A. H., and J. J. Yienger, 1996: Observed international variability in the Hadley circulation and its connection to ENSO. *J. Climate*, **9**(11), 275l–2767.

Qian, Y. F., S. Y. Wang, and H. Shao, 2001: A possible mechanism effecting the earlier onset of southwesterly monsoon in the South China Sea compared to the Indian monsoon. *Meteorology and Atmospheric Physics*, **76**, 237–250.

Ren, X. J., and Y. F. Qian, 2005: A coupled regional air-sea model, its performance and climate drift in simulation of the East Asian summer monsoon in 1998. *International Journal of Climatology Early View*, **25**, 679–692.

Wang, S. Y., and Y. F. Qian, 2001: Basic characteristic of surface heat field in 1998 and the possible connections with the SCS summer monsoon onset. *Acta Meteorologica Sinica*, **59**(1), 31–40. (in Chinese)

Wang, S. Y., and Y. F. Qian, 2002: The effects of vertical resolution of $p$-$\sigma$ coordinate regional climate model on simulated results. *Plateau Meteorology*, **20**(1), 28–35. (in Chinese)

Wu, B. Y., and R. H. Huang, 2001: Lag influences of winter circulations in the tropical western Pacific on South Asian summer monsoon. *Chinese Science Bulletin*, **46**(10), 858–861. (in Chinese)

Wu, G. X., and Y. S. Zhang, 1998: Tibetan Plateau forcing and the timing of the monsoon onset over South Asia and the South China Sea. *Mon. Wea. Rev.*, **126**(4), 913–927.

Wu, R., and B. Wang, 2001: Multi-stage onset of the summer monsoon over the western North Pacific. *Climate Dyn.*, **17**, 277–289.

Yao, Y. H., and Y. F. Qian, 2001: A study on the South China Sea monsoon index and the relationship between the index and regional rainfalls of China. *Journal of Nanjing University*, **37**(6), 781–788. (in Chinese)

Zhang, Y. C., and W. Perrie, 2001: Feedback mechanisms for the atmosphere and ocean surface. *Bound.-Layer Meteor.*, **100**, 321–348.